ACS Catalysis

Research Article

pubs.acs.org/acscatalysis

Correlating Hydrogen Oxidation/Evolution Reaction Activity with the Minority Weak Hydrogen-Binding Sites on Ir/C Catalysts

Jie Zheng, Zhongbin Zhuang, Bingjun Xu,* and Yushan Yan*

Department of Chemical and Biomolecular Engineering and Center for Catalytic Science and Technology, University of Delaware, 150 Academy Street, Newark, Delaware 19716, United States

Supporting Information

ABSTRACT: Fundamental understanding of the active sites mediating hydrogen oxidation/evolution reaction (HOR/HER) is critical to the design of an efficient HOR/HER electrocatalyst for affordable hydrogen exchange membrane fuel cells and electrolyzers. Here we report the existence of the most active sites on carbon supported iridium nanoparticles (Ir/C) for HOR/HER in alkaline electrolyte by investigating activities of Ir/C with varying particle sizes in the range of 3−12 nm. The distribution of surface sites is quantified by deconvoluting the H_{upd} desorption peak in cyclic voltammograms. The portion of the sites with the lowest hydrogen binding energy (HBE) increases with the increase of the particle size or the decrease of the total electrochemical active surface area (t-ECSA). The HOR/HER activity normalized to t-ECSA decreases as t-ECSA increases while it remains constant when normalized to the surface area of the sites with an average HBE of −0.33 eV, accounting for only about 15−30% of the total sites, shoulder the great majority of the HOR/HER activity.

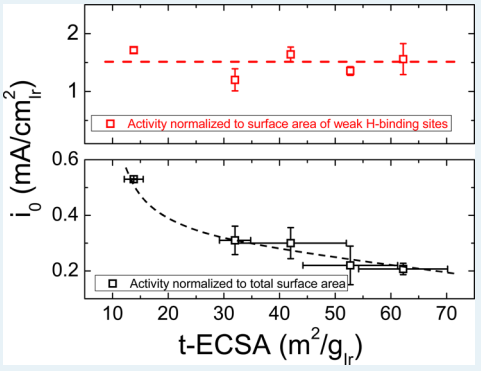

KEYWORDS: *hydrogen oxidation/evolution reaction, iridium nanoparticles, hydrogen binding energy, particle size effect, electrocatalysis*

INTRODUCTION

Hydrogen fuel cells have shown great promise to power next generation automobiles owing to their high energy efficiency and low environmental impact. The substantial cost reduction of proton exchange membrane fuel cells (PEMFCs)—generally constructed with Nafion membrane and Pt-based electrocatalysts—have set the stage for their future competition against internal combustion engines in automobiles, e.g., Toyota is scheduled to launch their PEMFC powered vehicles in 2015. However, the use of Pt-based catalysts in PEMFCs presents a severe barrier to their long-term economic competitiveness against internal combustion engines. Significant concerns also exist about whether there is sufficient room for further cost reductions. With the development of hydroxide exchange membranes (HEMs)[1,2] and nonprecious metal-based or even metal-free catalysts for oxygen reduction reaction (ORR) in alkaline electrolyte,[3−5] hydroxide exchange membrane fuel cells (HEMFCs)[6−9] have become an attractive alternative to PEMFCs. However, the activities of hydrogen oxidation/evolution reaction (HOR/HER) in alkaline electrolyte are about 2 orders of magnitude lower than that in acid on Pt, Pd, and Ir,[10,11] which makes the development of an effective HOR catalyst for HEMFCs a high priority. In addition, HER catalysts in alkaline electrolyzers face similar challenges.

Fundamental understanding for the sluggish kinetics of HOR/HER in the alkaline environment, the cornerstone for the rational design of efficient HOR/HER catalysts, remains a topic of considerable debate despite intense recent efforts.[10−15] A systematic study of HOR/HER activity on transition metals (Ag, Au, Cu, Pt, Pd, Co, Ni, Fe, and W) in bases reveals a volcano shaped curve when plotting the HOR/HER exchange current density vs the hydrogen binding energy (HBE) with Pt located at the optimal position, indicating that HBE is a key descriptor for catalytic activity for HOR/HER.[12] Meanwhile, Strmcnik et al. argued that the ability of metals to adsorb OH plays an important role in determining the HOR/HER activity, based on the excellent match between experimentally measured and simulated HOR/HER activity on Au, Pt, and Ir in the pH range of 1−13.[13] Later on, Durst et al. correlated the HBE inferred from cyclic voltammetry (CV) measurements with HOR activities, and the effect of pH on HOR/HER activity manifests itself by modifying the HBE of electrocatalysts, based on which HBE was proposed to be the "unique and sole" predictor for the performance of HOR/HER electrocatalysts.[11] Wang et al. showed the HOR/HER activity on PtRu/C is more than twice that of Pt/C, which is attributed to the lower HBE on PtRu as revealed by both CV measurements and density functional theory (DFT)-based calculations.[15] More recently, Sheng et al. correlated the HOR/HER activity on polycrystalline Pt to experimental

Received: February 5, 2015
Revised: May 19, 2015
Published: June 11, 2015

DOI: 10.1021/acscatal.5b00247
ACS Catal. 2015, 5, 4449−4455

measured HBE in electrolytes with pH from 0 to 13 and suggested HBE is the unique descriptor for HOR/HER.[16]

Considering that not all surface sites of a catalyst possess the same activity—for example, single crystal electrode studies show that different crystallographic facets of Pt exhibit drastically different HOR/HER activities[17,18]—identifying the most active sites is a key task for the rational design of better catalysts. Varying the size of metal nanoparticles offers a convenient approach to systematically tune the composition of sites with different local environments, e.g., terrace, edge, and corner sites.[19−22] In addition, surface sites with a variety of local environments can be sampled simultaneously with different particle sizes, which is not possible in the studies of single crystal surfaces. Active sites of HOR/HER can then be identified by correlating activities with their key properties, e.g., amount of sites with similar HBE. Strmcnik et al. reported that the HOR polarization curve on polycrystalline Ir in 0.1 M NaOH is essentially overlapping with the concentration overpotential curve, indicating a facile HOR/HER kinetics on polycrystalline Ir.[13] Thus, mechanistic understanding of the HOR/HER activity on Ir is of keen interest not only because it is a more cost-effective alternative to Pt (the average price for Pt and Ir during November 2013 to November 2014 is $1413.53 and $542.16/oz, respectively), but more importantly it could shed light on the guiding principles for the design of efficient nonprecious metal-based HOR/HER catalysts. Unlike the extensive research effort on Pt, HOR/HER kinetics studies on Ir are limited: most work was carried out in acidic electrolytes with potentially underestimated activity[23−25] and two in the alkaline environment.[11,13]

Herein, we present a detailed kinetic study of HOR/HER on Ir/C catalysts with varying Ir particle sizes (3−12 nm), which establishes the direct correlation of the HOR/HER activity with the lowest HBE minority sites on Ir/C. We first prove that the position of the under potential deposited H (H_{upd}) desorption peak is directly related to the HBE of the corresponding sites, followed by correlating the HOR/HER activity with the amount of sites with different HBEs. Exchange current density normalized by the electrochemical surface area (ECSA) corresponding to sites with H_{upd} desorption peak centered at 0.13 V vs RHE (or an HBE of −0.33 eV) was found to be independent of total electrochemical active surface area (t-ECSA) or particle size, indicating weak H-binding sites are likely the true active sites for HOR/HER. This finding suggests the design of efficient HOR/HER catalysts should aim at maximizing the density of weakly H-binding sites, rather than the total number of surface sites.

EXPERIMENTAL SECTION

Preparation and Characterization of Iridium Nanoparticle with Different Sizes. Ir/C samples with varying particle sizes were obtained by treating commercial 20 wt % Iridium on Vulcan XC-72 (Premetek Co.) in Ar at 300, 500, 600, and 800 °C for 2 h. The samples are referred to as Ir/C (untreated), Ir/C-300C, Ir/C-500C, Ir/C-600C, and Ir/C-800C, respectively. Their particle sizes and distributions were examined by a combination of high-resolution transmission electron microscopy (HRTEM), powder X-ray diffraction (XRD), and cyclic voltammetry (CV). TEM samples were prepared on TEM grid (Lacey carbon coated copper girds, Electron Microscopy Sciences) by adding a drop of sample suspended in isopropanol after being ultrasonicated for 5 min. The diameters of at least 300 Ir NPs of each sample were measured from TEM images (JEOL 2010F, 200 kV), and the number-averaged diameters were calculated. X-ray diffraction (XRD) patterns of each sample were recorded on a Philips X'Pert X-ray diffractometer using Cu Kα radiation.

Electrochemical Measurements. The electrochemical measurements were conducted using a three-electrode cell configuration, with silver−silver chloride (Ag/AgCl) as the reference electrode, Pt wire as the counter electrode, and a 5 mm diameter glassy carbon as the working electrode (PINE instruments) controlled by a multichannel potentiostat (Princeton Applied Research). All the potentials used in this work were converted to the reversible hydrogen electrode (RHE) calibrated from rotating disk electrode (RDE) measurement of hydrogen oxidation and evolution reactions. The Ir/C ink solutions were prepared by dispersing Ir/C in 0.05 wt % Nafion isopropanol solution to achieve an Ir weight concentration of 0.2 mg/mL. Isopropanol was chosen as the solution for better dispersion of the Ir/C catalysts, and Nafion was added as a binder. The thin-film electrodes were prepared by pipetting 5 μL of the catalysts ink twice onto glassy carbon electrodes which has been prepolished to a mirror finish with a final metal loading of 10 $\mu g_{Ir}/cm_{disk}^2$.

Cyclic voltammetry (CV) experiments were performed in Ar-saturated 0.1 M KOH solution (prepared from KOH pellets, 99.99% metal trace, Sigma-Aldrich) at a scanning rate of 50 mV/s from ∼0.01 to 1.0 V vs RHE without rotating. The electrochemical surface areas of Ir/C samples were determined from the hydrogen adsorption/desorption region with subtraction of double layer. The surface charge density of 218 $\mu C/cm_{Ir}^2$ was assumed for a monolayer adsorption of H on Ir.[26]

The HOR/HER activity measurements of all samples were performed in 0.1 M KOH solution saturated with H_2 at a scanning rate of 50 mV/s and a rotation speed of 1600 rpm for several cycles until a stable polarization curve was obtained. The scanning rate was then change to 1 mV/s, and this curve was reported in this paper. The *iR*-free potential was obtained after the correction of internal resistance measured by electrochemical impedance spectroscopy (EIS), and the correction equation is as follows

$$E_{iR\text{-free}} = E - iR \tag{1}$$

where E is the original potential, i is the corresponding current, R is the internal resistance, and $E_{iR\text{-free}}$ is the *iR*-free potential.

The electrochemical impedance spectroscopy measurement was performed from 200 kHz to 100 mHz right after the HOR/HER measurement.[10]

The kinetic current (i_k) of HOR was corrected using the following equation

$$\frac{1}{i} = \frac{1}{i_k} + \frac{1}{i_d} \tag{2}$$

where i is the measured current, i_k is the kinetic current, and i_d is the diffusion limited current defined as

$$\eta_{diffusion} = -\frac{RT}{2F}\ln\left(1 - \frac{i_d}{i_l}\right) \tag{3}$$

The exchange current density (i_0) of HOR/HER was obtained by fitting the kinetic current density into Butler−Volmer equation, which is

$$i_k = i_0\left[\exp\left(\frac{\alpha F\eta}{RT}\right) - \exp\left(\frac{(\alpha - 1)F\eta}{RT}\right)\right] \tag{4}$$

DOI: 10.1021/acscatal.5b00247
ACS Catal. 2015, 5, 4449−4455

Table 1. Number Averaged (d_n^{TEM}) and Volume/Area Averaged ($d_{v/a}^{TEM}$) Particle Size from TEM, Volume Averaged Particle Size from XRD (d_v^{XRD}), Surface Areas Calculated from $d_{v/a}^{TEM}$ ($S_{v/a}^{TEM}$), d_v^{XRD} (S_v^{XRD}), and Measured Electrochemically (S_v^{XRD})

	d_n^{TEM} (nm)	$d_{v/a}^{TEM}$ (nm)	d_v^{XRD} (nm)	$S_{v/a}^{TEM}$ (m^2/g_{Ir})	S_v^{XRD} (m^2/g_{Ir})	S^{EC} (m^2/g_{Ir})
Ir/C	2.86 ± 0.83	3.34	3.20	79.6	83.1	62.2 ± 8.0
Ir/C-300C	3.60 ± 0.60	4.24	3.94	62.7	67.5	52.7 ± 8.5
Ir/C-500C	5.01 ± 1.53	5.92	4.99	44.9	53.3	42.0 ± 15.4
Ir/C-600C	5.72 ± 2.30	7.62	8.06	34.9	33.0	32.0 ± 2.8
Ir/C-800C	7.04 ± 3.60	11.57	12.3	23.0	21.6	13.8 ± 1.7

where α is the transfer coefficient, F is the Faraday's constant (96 485 As/mol), η is the overpotential, R is the universal gas constant (8.314 J/(mol·K)), and T is temperature in Kelvin.

RESULTS

Effect of Particle Size on the Composition of Ir Sites. Carbon supported Ir catalysts with varying particle sizes were prepared by annealing commercial Ir/C at 300−800 °C in Ar. The average size of Ir particles increases with the annealing temperature. The number-average size (d_n^{TEM}) and size distribution, volume/area averaged size ($d_{v/a}^{TEM}$), and volume averaged particle size (d_v^{XRD}) of the Ir nanoparticles were determined by transmission electron microscopy (TEM) (Figure S1) and powder X-ray diffraction (XRD) (Figure S2) measurements. The value of $d_{v/a}^{TEM}$ is in good agreement with d_v^{XRD} (Table 1, data analysis protocols are detailed in the Supporting Information), indicating that the thermal treatment is a reliable method to obtain Ir particles in the range of 3−12 nm. Electrochemical active surface areas (ECSAs) obtained from cyclic voltammograms (S^{EC}) are smaller than those estimated from $d_{v/a}^{TEM}$ and d_v^{XRD} (Table 1), due to the contact of the particle with the support which are not accessible to CV measurements.

Supported Ir catalysts with different particle sizes have different composition of surface sites. There are three general features in the anodic branch of H_{upd} region in the cyclic voltammogram, indicating the Ir sites for the oxidation of H_{upd} are not homogeneous (Figure 1). This observation is reminiscent of the well-defined H_{upd} peaks assigned to the low-index crystallographic facets of Pt. However, the local environments of sites on supported Ir nanoparticles are much more diverse than single crystal surfaces, and the observed broad features should be interpreted as the manifestation of multiple groups of Ir sites sharing common properties key to HOR. We will show that the position of H_{upd} peak is directly correlated with the HBE of the corresponding sites via derivation in the Discussion section, as suggested by Durst et al. in a recent report.[11]

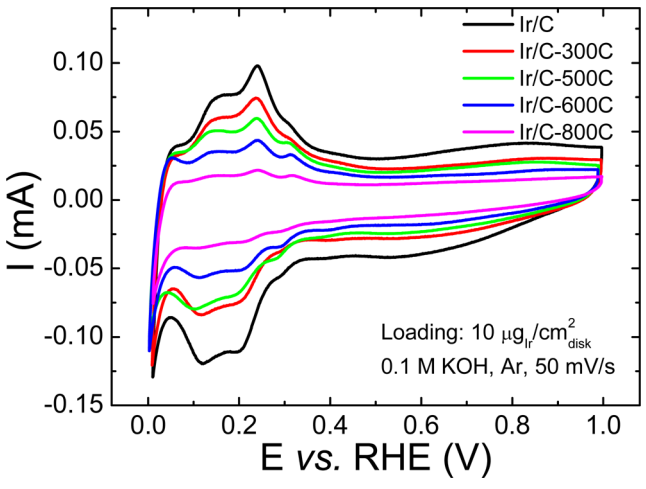

Figure 1. Cyclic voltammograms of Ir/C, Ir/C-300C, Ir/C-500C, Ir/C-600C, and Ir/C-800C conducted in Ar saturated 0.1 M KOH at a scan rate of 50 mV/s. The Ir loading for all samples is 10 $\mu g/cm_{disk}^2$.

HOR/HER Activity of Supported Ir Catalysts with Varying Particle Sizes. Key kinetic parameters of HOR/HER on Ir/C in alkaline electrolyte were obtained with a series of rotating disk electrode (RDE) measurements (Figure 2a−c). The HOR/HER polarization curve on Ir/C in 0.1 M KOH at 293 K (Figure 2a) reaches the max hydrogen mass transport limiting current density (i_l) at potentials above 0.2 V. Even after iR correction, the curve (red trace, Figure 2a) deviates significantly from concentration overpotential curve (blue dashed trace) which enables the quantification of its HOR/HER activity.[10,27] The kinetic current density (i_k) was obtained as described in the Experimental Section and fitted with the Butler−Volmer equation to determine the exchange current density (i_0) and transfer coefficient (α).

The fitted curve matches well with experimental data (Inset of Figure 2a), with i_0 and α being 0.21 ± 0.02 mA/cm^2_{Ir} and 0.56 ± 0.03, respectively. The i_l on the HOR/HER polarization curve increases as the rotation speed increases from 400 to 2500 rpm (Figure 2b). The i_l is proportional to the square root of rotating speed (ω, in radians per second), as indicated by the Levich equation, $i_l = 0.62nFD^{2/3}\nu^{-1/6}c_0\omega^{1/2} = Bc_0\omega^{1/2}$, where D is the diffusivity of hydrogen in 0.1 M KOH (3.7×10^{-5} cm^2/s), n is the number of electrons transferred in H_2 oxidation reaction (n = 2), ν is the kinematic viscosity of the electrolyte (1.01×10^{-2} cm^2/s (CRC handbook)) and c_0 is the solubility of H_2 in 0.1 M KOH (7.33×10^{-4} M) . The inverse of i_l at 0.25 V was plotted as a function of the inverse of $\omega^{1/2}$ (Inset of Figure 2b), which was linearly fitted to generate a line passing through the origin and a Bc_0 value of 0.0687 $mA/(cm^2_{disk}rpm^{1/2})$, in good agreement with calculated Bc_0 value (0.0678 $mA/(cm^2_{disk}rpm^{1/2})$). The HOR/HER polarization curves were measured at temperatures ranging from 275 to 313 K at 1600 rpm (Figure 2c). The i_l increases with temperature (Figure 2c), which is consistent with the report by Sheng et al. in the case of Pt(polycrystalline or pc).[10] The slope of the polarization curve becomes steeper with the increase of temperature, and the potential at which the limiting current was reached shifted negatively as temperature increases, indicating a faster kinetics of HOR/HER. The i_0 at different temperatures were extracted via the curve fitting to the Butler−Volmer equation, and an activation energy of 32.9 ± 1.5 kJ/mol was obtained by plotting $\ln(i_0)$ vs T^{-1} (Inset of Figure 2c), which is slightly higher than that on both Pt(pc) (28.9 ± 4.3 kJ/mol) and Pt/C (29.5 ± 4.0 kJ/mol).[10] Note that the i_0 we obtained at 313 K is 0.44 ± 0.03 mA/cm^2_{Ir}, in reasonable agreement with Durst et al.'s result on Ir.[11]

Kinetic studies of HOR/HER on Ir/C with varying particle sizes were performed (Figure S5). The exchange current density of supported Ir catalysts for HOR/HER decreases with the rise of t-ECSA (or the decrease of particle size), (Figure 2d and Table 2)

DOI: 10.1021/acscatal.5b00247
ACS Catal. 2015, 5, 4449−4455

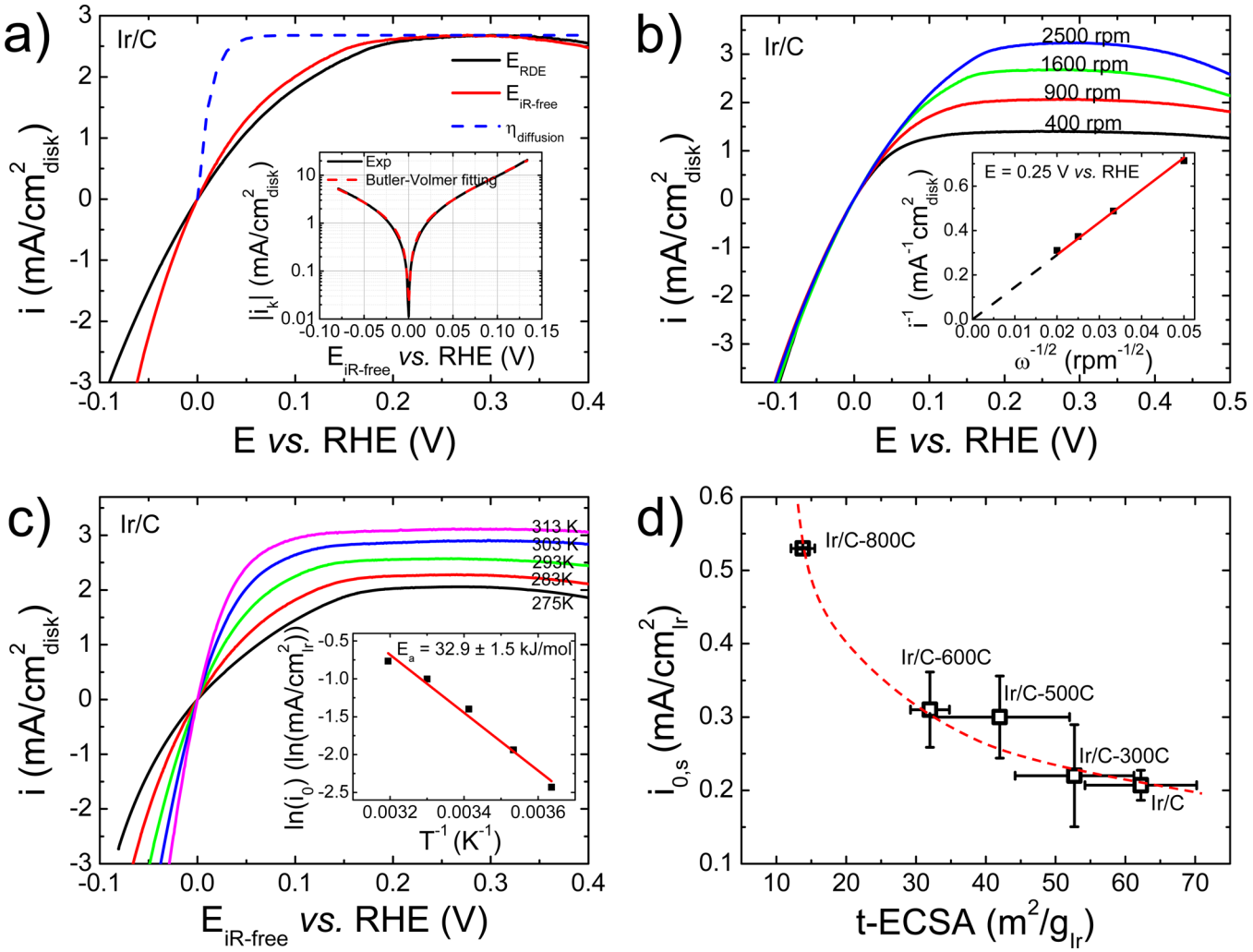

Figure 2. (a) HOR/HER polarization curve (positive scan) on Ir/C in 0.1 M KOH saturated with H_2 (1 atm) at a scan rate of 1 mV/s with a rotation speed of 1600 rpm at r.t. (293 K) before (black line) and after (red line) *iR* correction. The blue dashed line is the concentration overpotential curve. The loading of Ir was 10 $\mu g/cm_{disk}^2$. The inset shows the measured HOR/HER kinetic current density (black solid line) and the corresponding Butler–Volmer equation (eq 4) fitting (red dashed line) with $\alpha = 0.47$. (b) HOR/HER polarization curves on Ir/C in 0.1 M KOH saturated with H_2 (1 atm) at scan rate of 1 mV/s at r.t. with rotation speeds ranging from 400 to 2500 rpm. The inset shows a Koutecky–Levich plot at 0.25 V vs RHE. (c) HOR/HER polarization curves on Ir/C in 0.1 M KOH saturated with H_2 (1 atm) at a scan rate of 1 mV/s with a rotation speed of 1600 rpm at temperatures ranging from 275 to 313 K. The inset shows the Arrhenius plot with the slope corresponding to $-E_a/R$, giving an activation energy of 32.9 ± 1.5 kJ/mol. (d) Exchange current densities of HOR/HER on Ir/C samples normalized to t-ECSA as a function of t-ECSA. The red dashed line serves as the eye guiding line for the trend.

Table 2. Summary of average specific exchange current densities based on t-ECSA and mass exchange current densities of HOR/HER on all Ir samples and their corresponding transfer coefficients (α)

Samples	$i_{0,s}$ (mA/cm^2_{Ir})	$i_{0,m}$ (A/g_{Ir})	α
Ir/C	0.21 ± 0.02	128.6 ± 18.8	0.56 ± 0.03
Ir/C-300C	0.22 ± 0.07	110.3 ± 13.1	0.55 ± 0.02
Ir/C-500C	0.30 ± 0.06	118.4 ± 20.0	0.53 ± 0.03
Ir/C-600C	0.31 ± 0.05	97.8 ± 7.6	0.54 ± 0.02
Ir/C-800C	0.53 ± 0.01	73.0 ± 9.0	0.50 ± 0.01

suggesting that not all sites contributing to t-ECSA are equally active. All Ir/C samples have a similar transfer coefficient value (about 0.5), and in turn a Tafel slope of 116 mV/dec at 293 K, illustrating that their HOR/HER share the same mechanism. Strmcnik et al. obtained a polarization curve for HOR/HER that is essentially overlapped with the concentration overpotential curve of polycrystalline Ir (Ir(pc)) under similar conditions.[13] An analysis of the polarization curves as a function of exchange current density (Figure S6) reveals that when the exchange current density is a factor of 10 or higher than i_l – assuming a roughness factor of 1–significant overlap between the polarization and concentration overpotential curves exists. Based on this analysis, it can be inferred that the exchange current density of Ir(pc) should be at least 15 mA/cm^2 (for a roughness factor of 2) to 30 mA/cm^2 (for a roughness factor of 1), which agrees with our observed trend that the exchange current density increases with the particle size of Ir (Figure S7).

DISCUSSION

Correlating Hupd peaks in cyclic voltammogram with HBE of active sites. The position of H_{upd} desorption peaks in a cyclic voltammogram can be correlated with the HBE of the corresponding sites, as suggested by Durst et al.[11] Assuming a Langmuir isotherm, we show that the potential at the peak of

DOI: 10.1021/acscatal.5b00247
ACS Catal. 2015, 5, 4449–4455

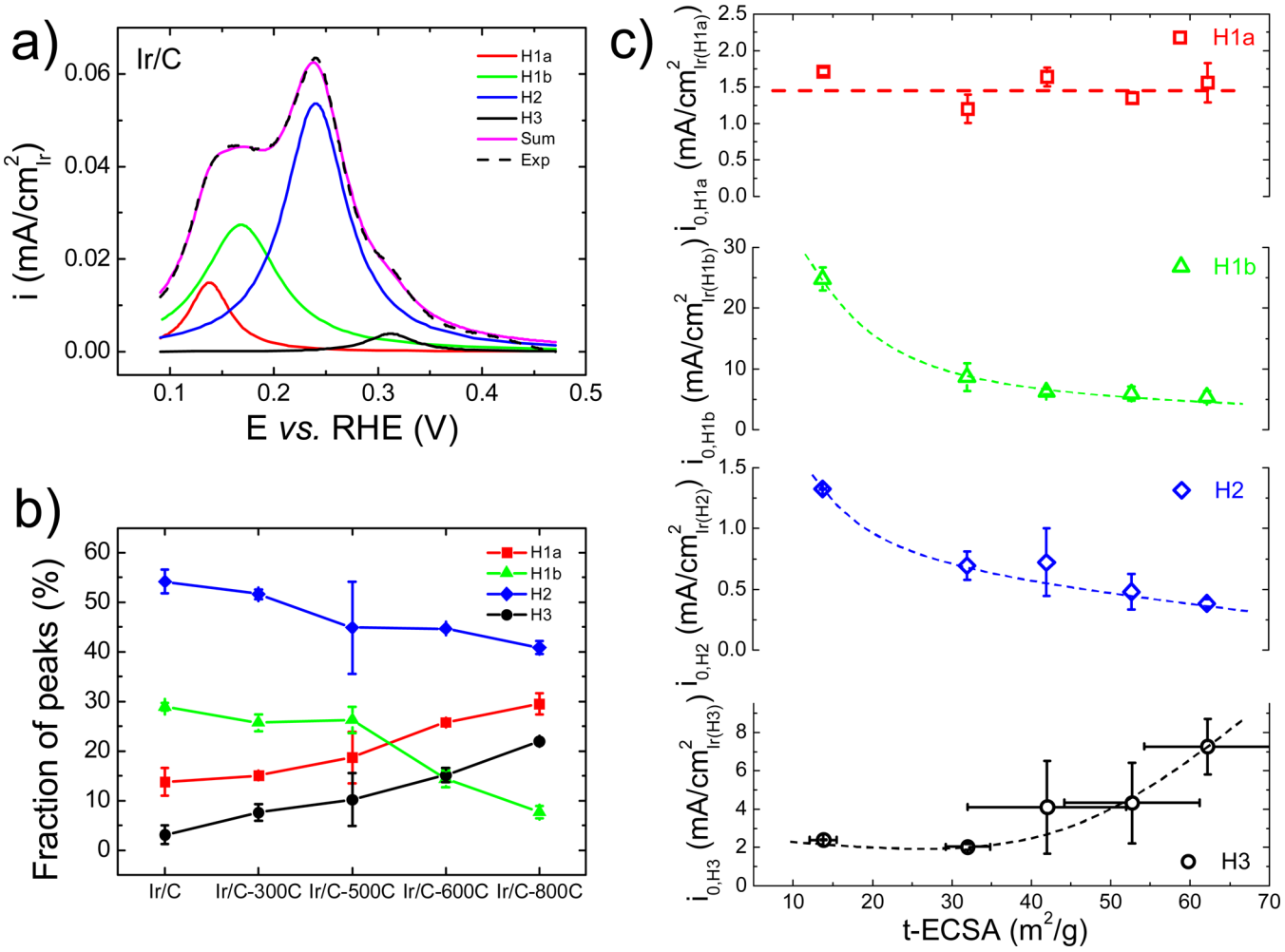

Figure 3. (a) Deconvolution of hydrogen desorption peaks into four peaks centered at 0.13 V (H1a), 0.18 V (H1b), 0.24 V(H2) and 0.32 V (H3) for Ir/C, (b) Fraction of peaks H1a, H1b, H2 and H3 among different samples, (c) i_0 normalized to surface area of H1a (peak potential 0.13 V), H1b (peak potential 0.18 V), H2 (peak potential 0.24 V) and H3 (peak potential 0.32 V) as a function of t-ECSA.

H_{upd} desorption features is related to the HBE of the corresponding sites through derivation by (Supporting Information and ref[16]):

$$E_{M-H} = -E_{peak}F - \frac{1}{2}TS^0_{H2} \quad (5)$$

in which E_{M-H}, E_{peak}, F, T, and S^0_{H2} are HBE of the metal sites, H_{upd} desorption peak potential vs RHE, Faraday's constant, temperature, and entropy of H_2 at standard conditions, respectively. The assumption that an equilibrium state is reached at each potential in CV testing used for the derivation is reasonable considering that H_{upd} adsorption and desorption is a fast process compared with the scanning rate, which can be verified by the minimal shift of peak potentials as the scanning rate decreases from 50 mV/s to 5 mV/s (Figure S4a). The shape of H_{upd} desorption peaks remains essentially unchanged within the range of scanning rate tested (Figure S4b) while the relative peak height of H_{upd} adsorption peak centered at ~0.13 V decreases as scanning rate decrease (Figure S4c). We hypothesize that the H_{upd} adsorption process is likely influenced by preadsorbed species while the H_{upd} desorption process is not. Therefore, the H_{upd} desorption regions are used for analysis. A E_{peak} value of 0.15 V for Pt(110) in 0.1 M $HClO_4$ yields the HBE of −33.6 kJ/mol, which is consistent with the reported value based on temperature-dependent cyclic voltammograms.[28] Studies also showed good agreements between the hydrogen adsorption energy in solution and in gas-phase.[29] The correlation between H_{upd} desorption peak position and HBE of the corresponding sites offers an easy and powerful approach to obtain structure−activity relation for HOR/HER. No detectable shift of H_{upd} desorption peak potentials (or HBE) of the different types of sites on Ir nanoparticles with varying particle sizes was observed. However, there is significant redistribution among those sites as particle size grows, as evidenced by the change in the cyclic voltammogram profile in the H_{upd} region on the anodic branch (Figure 1). It could be a key element in rationalizing the decreasing specific exchange current density for HOR/HER as t-ECSA increases (particle size decreases), since many reactions including HOR/HER are strongly structure sensitive.[17,18,30,31] For example, Marković et al. reported the HOR/HER exchange current densities on three Pt single crystals in the order of (110) > (100) > (111) in both acidic[18] and alkaline[17] electrolytes. In addition, Kinoshita et al. observed an increased ratio between the amount of "strongly" adsorbed hydrogen and "weakly" adsorbed hydrogen as Pt particle size increases in both H_2SO_4[32,33] and NaOH[33] electrolytes, which was attributed to the change in fractions of different facets as particle size varies.

DOI: 10.1021/acscatal.5b00247
ACS Catal. 2015, 5, 4449−4455

Identifying true active sites for HOR/HER via peak deconvolution. To gain a more quantitative understanding of the effect of Ir particle size on HOR/HER activity in alkaline electrolyte, the H_{upd} desorption profiles were deconvoluted into multiple peaks to quantify the site distribution followed by correlating the measured HOR/HER activities to the amount of each sites. H_{upd} desorption region with potential greater than 0.09 V vs RHE was chosen where the impact of a slight HOR current resulted from absence of rotating or a small variation of the lowest potential limit in CV is negligible (Figure S3a,b). Initially, the H_{upd} desorption profiles were deconvoluted into three naturally existed peaks centered at 0.16 V (H1), 0.24 V (H2) and 0.32 V (H3), respectively (Figure S8). However, we were unable to obtain good peak fitting with identical peak widths (fwhm) for each species (H1, H2 and H3), indicating the heterogeneous nature of the sites within each species (Table S1). In addition, sites corresponding to H1 have lower overpotential for HOR than H2 and H3 by 0.08 and 0.16 V, respectively. Then, the HOR rate constant mediated by H1 should be a factor of 24 and 565 faster than that of H2 and H3, respectively, assuming identical preexponential factors in the Arrhenius eq (Supporting Information). It follows that the exchange current density normalized by the fraction of H1 ($i_{0,H1}$) in all sites should be independent of particle size or t-ECSA if sites corresponding to H1 are true active sites for HOR/HER. Figure S9b shows that $i_{0,H1}$ decreases with increasing t-ECSA (decreasing particle size), suggesting H1 is not a truthful representation of active sites. We attribute the poor correlation between H1 and HOR/HER activity to the heterogeneity of sites corresponding to H1, and hypothesize that a fraction of sites in H1 with lower HBE are the true active sites although two subpeaks of H1 cannot be resolved even at a scanning rate as low as 5 mV/s (Figure S4).

We further deconvoluted H1 into H1a and H1b centered at 0.13 and 0.18 V, respectively, and for all samples, the measured HOR/HER activities correlates well with sites corresponding to H1a (Figure S11). We fixed the peak width of H1b, H2, and H3 in the fitting, and the best fitting was achieved when the peak width of H1a grows slightly with particle size, reflecting a small degree of heterogeneity of H1a sites (Figure 3a, Figure S10 and Table S2). No further deconvolution of H1a peak was attempted because reasonable structure−activity correlation can be extracted with H1a and H1b. The fractions of H1a and H3 sites increase as particle size grows, while the opposite is true for H1b and H2, indicating that H1a and H3 sites are likely terrace sites. Among the four types of sites, H1a sites has the lowest HBE and, hence, corresponds to most weakly bound H_{upd}. When the exchange current densities were normalized to the surface area of H1a, H1b, H2, and H3, respectively (denoted as $i_{0,H1a}$, $i_{0,H1b}$, $i_{0,H2}$, and $i_{0,H3}$), $i_{0,H1a}$ becomes independent of t-ECSA while $i_{0,H1b}$, $i_{0,H2}$, and $i_{0,H3}$ either increase or decrease with t-ECSA (Figure 3), which provides the following key mechanistic insights: (1) Only Ir sites corresponding to H1a contribute significantly to HOR/HER activity. (2) A small fraction (15−30%) of active Ir sites shoulder most of the HOR activity, suggesting that increasing the density of those sites rather than total Ir sites should be the strategy in the design of future Ir-based HOR catalysts. It is consistent with the estimation that the HOR rate constant for H1a sites will be a factor of 7.2 higher than that of sites corresponding to H1b (Supporting Information). We also simulated the exchange current density based on weighed addition of the four peaks: the simulated exchange current densities agree well the experimental ones, with the majority of the activity contributed from sites associated with peak H1a (Figure S12), indicating peak H1a sites are the most active ones. (3) Ir sites on low index planes are more likely to be the active sites for HOR (H1a) since the fraction of low index planes typically increases as particle size grows. This can be inferred by comparing the plot of peak H1a, H1b, H2, and H3 fractions for different-sized Ir/C samples (Figure 2b) and the simulated surface distribution of a cuboctahedron structure (Figure S13). Although a uniform charge density was used to calculate the electrochemical surface area while different facets likely have different charge densities, the relation between $i_{0,H1a}$, $i_{0,H1b}$, $i_{0,H2}$, $i_{0,H3}$, and t-ECSA does not change (only the absolute values of $i_{0,H1a}$, $i_{0,H1b}$, $i_{0,H2}$, and $i_{0,H3}$ are adjusted by a constant) based on derivation shown in the Supporting Information. The hydrogen adsorption and desorption on single crystal Ir were studied by Motoo et al. where different hydrogen desorption peak potentials were observed for the three low index facets in the order of (110) < (111) < (100) in 0.1 M $HClO_4$.[34] More positive hydrogen desorption peak potentials were observed on high index Ir facets as compared with Ir(110) and Ir(111) by Furuya et al.,[35] indicating a higher hydrogen binding energy on high index Ir facets. In addition, it is also consistent with the report by Strmcnik et al. that polycrystalline Ir disk exhibits very high HOR activity,[13] in that Ir disk contains higher density of low index planes than nanoparticles. Furthermore, the coordination number for Ir atoms on low index planes is higher than that of defective surfaces, which typically leads to lower binding to adsorbates. The increasing trend of peak H3 with particle size seems to suggest the sites associated with peak H3 might also be certain type of low-coordinate site with a high HBE. Similar phenomenon has been observed on Pt/C that the H_{upd} desorption peak with highest HBE arises as particle size increases.[36] However, more detailed investigations on single crystalline Ir surfaces for accurate peak assignments will be the subject of future studies.

The excellent correlation between sites with lowest HBE and the HOR/HER activity supports the hypothesis that HBE is the key descriptor for HOR/HER catalysts, as argued by Durst et al.,[11] Sheng et al.,[16] and Wang et al.[15] It was hypothesized that Pt showed much lower HOR/HER activity in alkaline electrolyte than that in acid mainly due to its higher HBE in the alkaline environment. Similarly, it has been shown by Durst et al.[11] and our own work (Figure S14a) that Ir have more positive H_{upd} desorption peak potential in alkaline than in acid electrolyte, revealing the HBE of Ir is also higher in alkaline than in acidic media. Iridium has been grouped in the weak hydrogen binding branch in the volcano plot for acidic electrolyte.[37] If we consider that Ir has an inferior HOR/HER activity than Pt simply due to its weaker HBE than Pt in acid, then one would expect an increase of HOR/HER activity on Ir in alkaline electrolyte due to the stronger HBE in alkaline electrolyte. However, our measurement by RDE method of Ir/C in 0.1 M $HClO_4$ using a loading of 10 $\mu g_{Ir}/cm_{disk}$ showed an overlapping of the polarization curve with the concentration overpotential curve (Figure S14b), indicating a much faster HOR/HER kinetic on Ir in acid than in base. The HOR/HER activity of Ir/C at 313 K measured using H_2-pump with proton exchange membrane (which mimics the acidic environment) is 120 times of that in 0.1 M NaOH,[11] which agrees with our result. These experimental observations suggest that Ir also belongs to the branch with too strong HBE, and it follows that sites with lower HBE will have higher HOR/HER activity.

DOI: 10.1021/acscatal.5b00247
ACS Catal. 2015, 5, 4449−4455

CONCLUSION

In conclusion, we studied the HOR/HER kinetics on Ir/C in alkaline electrolyte systematically using a thin-film RDE method. By tuning the Ir particle size from 3 to 12 nm, we were able to vary the surface site distribution quantified by deconvolution analysis on the H_{upd} desorption region of CVs: the population of the sites with smallest HBE (higher HOR/HER activity) increases as particle size increase. Particle size effect of HOR/HER on Ir/C was observed: the specific HOR/HER activities (activity normalized to t-ECSA) decrease as t-ECSA increases (or particle size decreases). HOR/HER activities normalized to the surface area of the lowest hydrogen binding site are independent of t-ECSA, indicating that those sites with low HBE (most likely low-index facets) are the most active sites for HOR/HER. Therefore, our study suggests that extended Ir nanostructure with high fraction of low-index facets such as Ir nanotubes or nanowires may have higher HOR/HER activities compared with small Ir nanoparticles.

ASSOCIATED CONTENT

Supporting Information

The Supporting Information is available free of charge on the ACS Publications website at DOI: 10.1021/acscatal.5b00247.

Transmission electron microscopy (TEM) images, X-ray diffraction (XRD) patterns, hydrogen oxidation/evolution polarization curves of all Ir samples, and deconvolution of H_{upd} desorption peaks (PDF)

AUTHOR INFORMATION

Corresponding Authors

*E-mail: yanys@udel.edu (Y.S.Y.).
*E-mail: bxu@udel.edu (B.X.).

Notes

The authors declare no competing financial interest.

ACKNOWLEDGMENTS

We acknowledge the partial support by the U.S. Department of Energy through the ARPA-E Program under No. DE-AR0000009 and the Fuel Cell Technologies Program under No. DE-AC52-06-NA25396 with the Los Alamos National Laboratory and the University of Delaware. We greatly thank Dr. Wenchao Sheng for training on electrochemical techniques and useful discussion.

REFERENCES

(1) Pan, J.; Chen, C.; Zhuang, L.; Lu, J. *Acc. Chem. Res.* **2012**, *45*, 473−481.
(2) Varcoe, J. R.; Atanassov, P.; Dekel, D. R.; Herring, A. M.; Hickner, M. A.; Kohl, P. A.; Kucernak, A. R.; Mustain, W. E.; Nijmeijer, K.; Scott, K.; Xu, T.; Zhuang, L. *Energy Environ. Sci.* **2014**, *7*, 3135−3191.
(3) Piana, M.; Catanorchi, S.; Gasteiger, H. A. *ECS Trans.* **2008**, *16*, 2045−2055.
(4) Suntivich, J.; Gasteiger, H. A.; Yabuuchi, N.; Nakanishi, H.; Goodenough, J. B.; Shao-Horn, Y. *Nat. Chem.* **2011**, *3*, 546−550.
(5) Chung, H. T.; Won, J. H.; Zelenay, P. *Nat. Commun.* **2013**, *4*, 1922.
(6) Filpi, A.; Boccia, M.; Gasteiger, H. A. *ECS Trans.* **2008**, *16*, 1835−1845.
(7) Lu, S.; Pan, J.; Huang, A.; Zhuang, L.; Lu, J. *Proc. Natl. Acad. Sci. U. S. A.* **2008**, *105*, 20611.
(8) Piana, M.; Boccia, M.; Filpi, A.; Flammia, E.; Miller, H. A.; Orsini, M.; Salusti, F.; Santiccioli, S.; Ciardelli, F.; Pucci, A. *J. Power Sources* **2010**, *195*, 5875−5881.
(9) Gu, S.; Sheng, W.; Cai, R.; Alia, S. M.; Song, S.; Jensen, K. O.; Yan, Y. *Chem. Commun.* **2013**, *49*, 131−133.
(10) Sheng, W.; Gasteiger, H. A.; Shao-Horn, Y. *J. Electrochem. Soc.* **2010**, *157*, B1529−B1536.
(11) Durst, J.; Siebel, A.; Simon, C.; Hasche, F.; Herranz, J.; Gasteiger, H. A. *Energy Environ. Sci.* **2014**, *7*, 2255−2260.
(12) Sheng, W.; Myint, M.; Chen, J. G.; Yan, Y. *Energy Environ. Sci.* **2013**, *6*, 1509−1512.
(13) Strmcnik, D.; Uchimura, M.; Wang, C.; Subbaraman, R.; Danilovic, N.; van der Vliet, D.; Paulikas, A. P.; Stamenkovic, V. R.; Markovic, N. M. *Nat. Chem.* **2013**, *5*, 300−306.
(14) Sheng, W.; Bivens, A. P.; Myint, M.; Zhuang, Z.; Forest, R. V.; Fang, Q.; Chen, J. G.; Yan, Y. *Energy Environ. Sci.* **2014**, *7*, 1719−1724.
(15) Wang, Y.; Wang, G.; Li, G.; Huang, B.; Pan, J.; Liu, Q.; Han, J.; Xiao, L.; Lu, J.; Zhuang, L. *Energy Environ. Sci.* **2015**, *8*, 177−181.
(16) Sheng, W.; Zhuang, Z.; Gao, M.; Zheng, J.; Chen, J. G.; Yan, Y. *Nat. Commun.* **2015**, *6*, 5848.
(17) Marković, N. M.; Sarraf, S. T.; Gasteiger, H. A.; Ross, P. N. *J. Chem. Soc., Faraday Trans.* **1996**, *92*, 3719−3725.
(18) Marković, N. M.; Grgur, B. N.; Ross, P. N. *J. Phys. Chem. B* **1997**, *101*, 5405−5413.
(19) Mukerjee, S. *J. Appl. Electrochem.* **1990**, *20*, 537−548.
(20) Jaramillo, T. F.; Jørgensen, K. P.; Bonde, J.; Nielsen, J. H.; Horch, S.; Chorkendorff, I. *Science* **2007**, *317*, 100−102.
(21) Maillard, F.; Pronkin, S.; Savinova, E. R. In *Handbook of Fuel Cells*; John Wiley & Sons, Ltd: Chichester, UK, 2010; DOI: 10.1002/9780470974001.f500002a.
(22) Nesselberger, M.; Ashton, S.; Meier, J. C.; Katsounaros, I.; Mayrhofer, K. J. J.; Arenz, M. *J. Am. Chem. Soc.* **2011**, *133*, 17428−17433.
(23) Trasatti, S. *J. Electroanal. Chem. Interfacial Electrochem.* **1972**, *39*, 163−184.
(24) Zoski, C. G. *J. Phys. Chem. B* **2003**, *107*, 6401−6405.
(25) Montero, M. A.; Fernández, J. L.; Gennero de Chialvo, M. R.; Chialvo, A. C. *J. Phys. Chem. C* **2013**, *117*, 25269−25275.
(26) Woods, R. *J. Electroanal. Chem. Interfacial Electrochem.* **1974**, *49*, 217−226.
(27) Gasteiger, H. A.; Markovic, N. M.; Ross, P. N. *J. Phys. Chem.* **1995**, *99*, 8290−8301.
(28) Jerkiewicz, G. *Prog. Surf. Sci.* **1998**, *57*, 137−186.
(29) Jerkiewicz, G.; Zolfaghari, A. *J. Electrochem. Soc.* **1996**, *143*, 1240−1248.
(30) Herrero, E.; Franaszczuk, K.; Wieckowski, A. *J. Phys. Chem.* **1994**, *98*, 5074−5083.
(31) Perez, J.; Villullas, H. M.; Gonzalez, E. R. *J. Electroanal. Chem.* **1997**, *435*, 179−187.
(32) Kinoshita, K.; Lundquist, J.; Stonehart, P. *J. Catal.* **1973**, *31*, 325−334.
(33) Kinoshita, K.; Ferrier, D. R.; Stonehart, P. *Electrochim. Acta* **1978**, *23*, 45−54.
(34) Motoo, S.; Furuya, N. *J. Electroanal. Chem. Interfacial Electrochem.* **1984**, *181*, 301−305.
(35) Furuya, N.; Koide, S. *Surf. Sci.* **1990**, *226*, 221−225.
(36) Sun, Y.; Dai, Y.; Liu, Y.; Chen, S. *Phys. Chem. Chem. Phys.* **2012**, *14*, 2278−2285.
(37) Norskov, J. K.; Bligaard, T.; Logadottir, A.; Kitchin, J. R.; Chen, J. G.; Pandelov, S. *J. Electrochem. Soc.* **2005**, *152*, J23−J26.

DOI: 10.1021/acscatal.5b00247
ACS Catal. 2015, 5, 4449−4455